JOC The Journal of Organic Chemistry

Article

pubs.acs.org/joc

PAMAM Dendrimer-Induced Aggregation of 5(6)-Carboxyfluorescein

Marco Bonizzoni, S. Reid Long, Chance Rainwater, and Eric V. Anslyn*

Department of Chemistry and Biochemistry, The University of Texas at Austin, 100 E. 24th St. A1590, Austin, Texas 78712, United States

Supporting Information

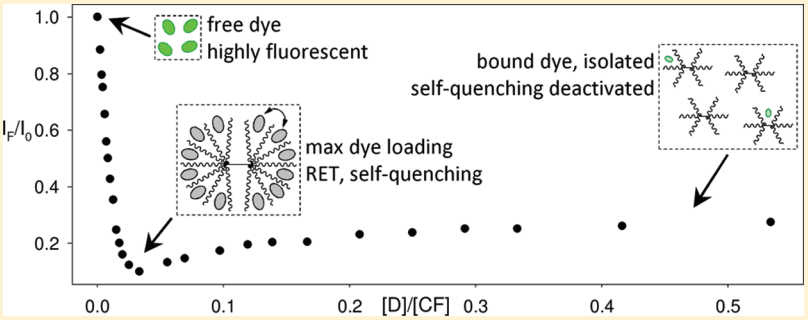

ABSTRACT: The binding of the fluorescent polyanionic probe 5(6)-carboxyfluorescein (**CF**) to various generations of dendrimers (**G3**−**G7**) was studied in buffered aqueous media by absorbance and fluorescence spectroscopy and by isothermal titration calorimetry (ITC). Absorbance, fluorescence, and fluorescence anisotropy data were collected concurrently by using a multiwell plate format. Because ITC does not depend on the presence of a chromophore/fluorophore for measurement, it allowed the exploration of concentration ratios otherwise unattainable in the spectroscopy experiments. Qualitative dendrimer generational trends were observed and found to be consistent with dendrimer size and charge. However, a number of significant anomalies were found in the spectroscopic titration profiles, which led us to propose a binding model comprising multiple, concurrent binding regimes. The predictive value of the model was ascertained by construction of a binding simulation, which was consistent with the experimental results. Finally, ITC results afforded insights into the fundamental thermodynamic properties of the binding process along with trends found across dendrimer generations. Thermodynamic data were found to be in accordance with the proposed model.

INTRODUCTION

The assembly of functional macrostructures in water that are derived from small-molecule building blocks has potential applications in catalysis and sensing.[1] For this purpose, we have been studying the high-stoichiometry anion sequestration by amine-terminated poly(amidoamine) (PAMAM) dendrimers with an ethylenediamine core. These macrostructures are soluble in buffered aqueous solution near neutral pH and are polycations as a result of the protonation of a sizable fraction of the surface amine groups.[2] Thus, they provide large, yet water-soluble, organic scaffolds with uniform primary interaction points (i.e., the surface ammonium groups) for electrostatically driven anion assembly. Due to the multivalency of the scaffold, these electrostatic interactions are thermodynamically quite favorable, yet they are also very labile, thus providing a regime of fast guest exchange. In addition, PAMAM dendrimers are stable over a wide range of pH values;[3] however, they do not have any UV−vis spectroscopy signatures, making them optically silent in the assembly process. These considerations led us to establish a method for monitoring binding processes by using the small spectroscopically active probe, 5(6)-carboxyfluorescein (**CF**), which is the focus of this report.

Previous studies aimed at investigating the high-stoichiometry binding characteristics of PAMAM dendrimers have been reported in the literature, e.g., by the Ford and Bryszewska groups,[4] by the Gröhn group,[4c] and also by this group,[5] among others, but to our knowledge a comprehensive study of these interactions comparing spectroscopic and calorimetric results across dendrimer families has not yet been carried out, nor has an interpretative model been proposed. For instance, the Gröhn group has previously studied the interaction of sulfonated anionic chromophores with G4 PAMAM dendrimers through UV−vis spectroscopy and ITC measurements, but they did not extend their study to fluorescence or to the effects of increasing size and surface charge across dendrimer generations.

In this study, 5(6)-carboxyfluorescein was used as a fluorescent probe to investigate anion binding to dendrimer scaffolds and the existence of binding trends across dendrimer generations. **CF** is a readily available, inexpensive, and reasonably bright water-soluble fluorophore that bears 2 to 3 negative charges in aqueous solutions at neutral pH, as shown in eq 1.[6] In addition, a very significant difference in rotational correlation lifetime was expected for this probe between the free state in solution and a dendrimer-bound state. This expected

Received: June 29, 2011
Published: December 6, 2011

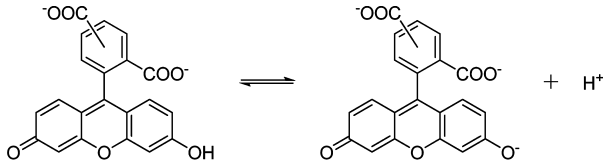

5(6)-carboxyfluorescein (**CF**)

change is ascribable to the difference in molar masses between the free dye in solution and the dendrimer−dye complex. Thus, a marked change in the fluorescence anisotropy of **CF** was expected upon interaction, which we herein report provides a clean, reliable, and sensitive binding signal.

Commercially available PAMAM dendrimer generations **G4**−**G7** were investigated (Table 1). The molar mass of the dendrimer molecules roughly doubles with each generational step. The table shows that the higher generation dendrimers display higher positive surface charge density, which can be expected to induce stronger electrostatic interactions with negatively charged species. Generations lower than 4 were deemed too small to act as useful scaffolds. On the other hand, commercially available generations higher than 7, although promising in principle, were simply too costly to realistically propose their use as general purpose off-the-shelf scaffolds and therefore were not considered in this study.

Table 1. Selected Molecular Properties of the Amine Terminated PAMAM Dendrimers Used in This Study[3,7]

generation	M_w (kDa)	diameter (Å)	surface NH_2	surface charges
G4	14.2	45	64	~31
G5	28.8	54	128	~64
G6	58.0	67	256	~115
G7	116.5	81	512	~256

Since this study looks at the interaction of large cationic dendrimers with smaller organic anions, we felt it interesting to look at the number of surface charges for the dendrimers. The protonation of amine-terminated PAMAM dendrimers has been studied through potentiometric titrations by the Borkovec group, and the number of surface charges can be estimated from the published results.[3] At pH 7.5 in a solution with ionic strength I = 0.1 M, the degree of protonation was found to be very close to ~50% for generations **G4**−**G6** and almost independent of the dendrimer generation. These results are in conformity with the "large molecule limit" characteristic of the titration curves of high molecular weight polyelectrolytes.[3] In the following discussion, we will also assume that the degree of protonation follows the experimental and estimated values reported in Table 1. However, the exact number of positive charges on the surface of the dendrimer is not of the utmost importance to our experiments; the doubling trend across generations will be the most important factor we rely upon in our interpretation.

RESULTS AND DISCUSSION

All of the following spectroscopic measurements were conducted in aqueous solutions containing 50 mM HEPES and buffered to pH 7.4.

Absorbance Measurements. In accordance with its initial spectral signature (absorption λ_{max}, molar extinction coefficient), we can assume that in our experimental conditions the fluorophore is completely deprotonated and bears three negative charges (eq 1). This is supported by the fact that the pK_a of **CF** is 6.5 and our operating pH is 7.4. Upon addition of PAMAM dendrimers to **CF**, a red shift in the absorption occurs (Figure 1). This behavior was common to all generations (Figure 2). The isotherms all share comparable end points, indicating that in its final bound state the small dye experiences the same immediate molecular environment no matter what generation of dendrimer it is bound to. However, increasingly high amounts of the lower generation dendrimers are required to lead to full sequestration of the **CF** (see inset Figure 2).

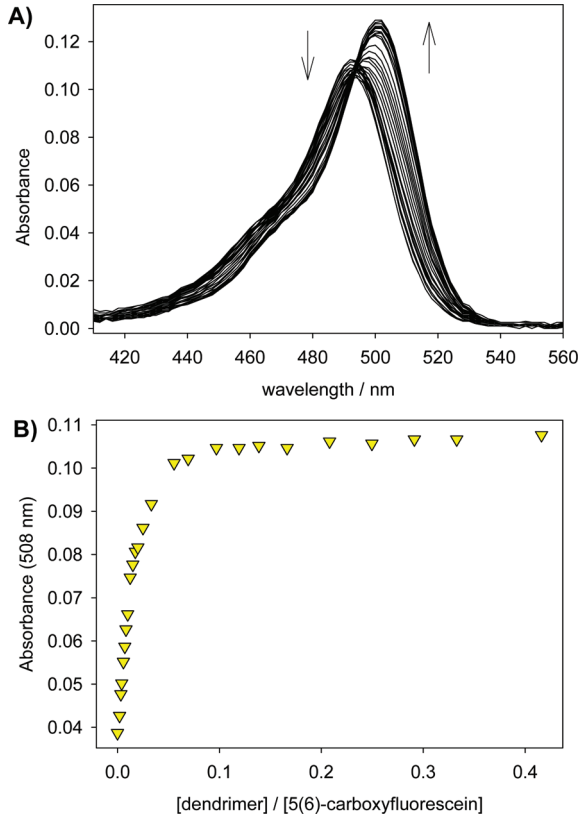

Figure 1. Titration of 5(6)-carboxyfluorescein (**CF**) with amine-terminated **G7** PAMAM dendrimer. (A) Family of absorbance spectra. (B) Absorbance isotherms observed from the titration in panel A.

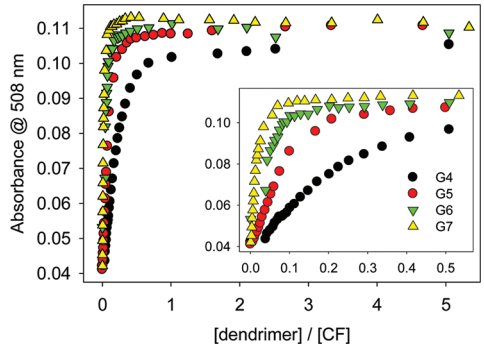

Figure 2. Generational trends in the absorbance signal: comparison between isotherms obtained from the interaction of 5(6)-carboxyfluorescein (**CF**) with PAMAM dendrimers of generations **G4**−**G7**, in buffered H_2O (50 mM HEPES at pH 7.4). [**CF**] = 2.0 × 10^{-6} M. Inset: a detail of the region of low [dendrimer]/[**CF**].

Binding of the anionic dye to the dendrimer is likely to be primarily driven by electrostatic interactions, but cation-π interactions between the aromatic core of the dye and the surface

dx.doi.org/10.1021/jo201360u | J. Org. Chem. 2012, 77, 1258−1266

ammonium group of the dendrimer may play a secondary role in stabilizing the complexes. Ammonium-arene interactions are known to be energetically significant even in aqueous solvents, as shown by Dougherty.[8] Irrespective of the driving force for binding, it is reasonable to assume that the polarity of the dye's ground and excited states are different. In particular, since we can safely assume that the excited state of the dye is more highly polar than the ground state, due to some degree of internal charge transfer, in a bound dye molecule the former will be more strongly stabilized by electrostatics and/or cation-π interactions. As a consequence, the HOMO−LUMO gap energy is reduced upon binding, thus causing the observed red shift in the absorption spectra.

Lastly, it should be noted that signal saturation is reached at far less than 1 equiv of dendrimer, which means there is a high stoichiometry of binding **CF** to the dendrimer generations. This observation will be discussed in further detail below.

Fluorescence Data. Fluorescence intensity and anisotropy data were collected concurrently with the absorbance spectra. The degree of polarization in the emitted light after excitation with linearly polarized light (fluorescence anisotropy for short) is strictly correlated with the rate of rotational diffusion of the emitter. Small molecules have fast rotational diffusion rates, which translates to low fluorescence anisotropy values, while larger and heavier molecules or complexes tumble much more slowly, resulting in an increased anisotropy signal. In the present context, the rotational diffusion lifetime of the dye changes drastically between its two states in solution, i.e., free and bound to a dendrimer. The unbound fluorophore has a very short rotational diffusion lifetime (i.e., its tumbling motion is very fast). Once bound to a dendrimer, however, the fluorophore assumes the tumbling rate of the dendrimer-dye complex, which is mainly dictated by the large dendrimer it is bound to. As a consequence, its fluorescence anisotropy signal is very high. Thus, we looked at fluorescence anisotropy as a reporter of binding. Experimental noise was estimated by measuring the fluorescence intensity of wells containing only buffer. By subtracting these "blanks" from the fluorescence intensity measurements, we virtually eliminated any reproducibility differences due to plate-to-plate variability and instrument-derived systematic errors. This was done for both the intensity and anisotropy data.

As the ratio of dendrimer to fluorophore was increased, the intensity of the fluorescence decreased very sharply, and only a fraction of an equivalent of dendrimer was necessary to trigger this response. Upon further increase of dendrimer content, however, a portion of the quenched fluorescence emission was recovered. In the presence of a large excess of dendrimer, the final fluorescence measurements level to a plateau that represents partial quenching of the **CF** emission by the dendrimer. The complex titration behavior is displayed by all dendrimer generations, albeit to varying degrees. Figure 3 shows a superimposition of isotherms obtained from dendrimers of **G4**−**G7**.

As can be seen in Figure 3A, the fluorescence spectra reach the same plateau independent of the dendrimer generation. When there is more than 1 equiv of dendrimer, each **CF** on average would find itself bound to a single dendrimer. Hence, the final fluorescence quenching caused by the dendrimers is independent of generation. The quenching is most likely due to photoinduced electron transfer (PET) from the tertiary amines in the interior of the dendrimer scaffold. This quenching is indicative of binding of **CF** to the dendrimer, and the complex behavior of the titration isotherm at the very low stoichiometry

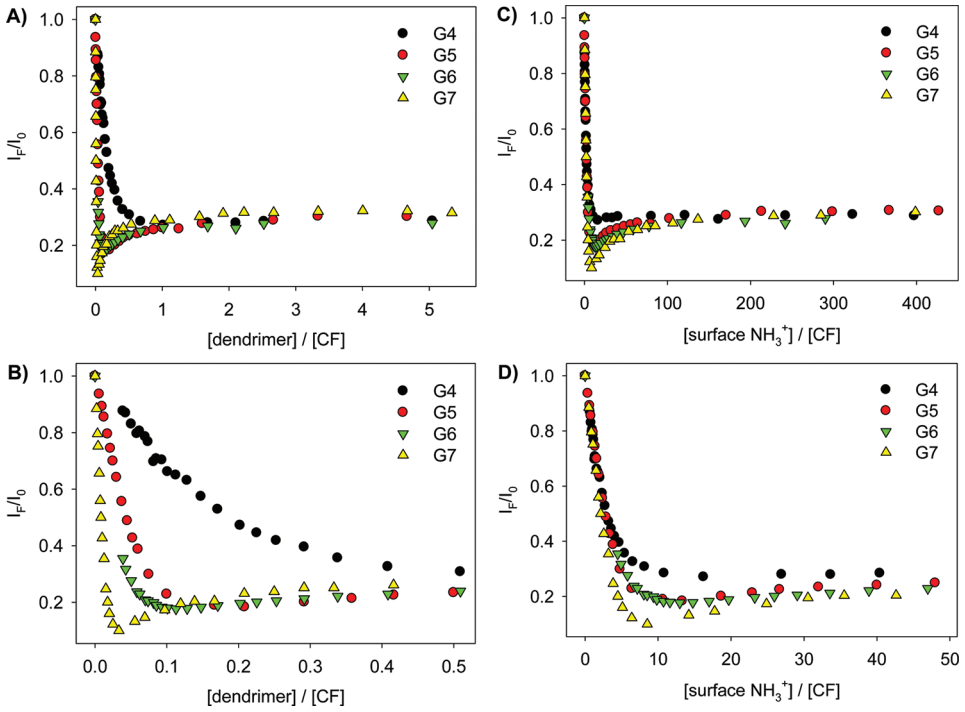

Figure 3. Overlay of fluorescence intensity isotherms obtained during the course of titrations of solutions of 5(6)-carboxyfluorescein (**CF**) with **G4**−**G7** amine-terminated PAMAM dendrimer in buffered H_2O (50 mM HEPES at pH 7.4). [**CF**] = 2.0×10^{-6} M. (A) Data plotted over the full concentration scale. (B) Detail of the maximum quenching region. (C) Data plotted as a function of the relative concentration of ammonium groups, over the full concentration range. (D) Detail of the maximum quenching region, as a function of the relative concentration of ammonium groups. Vertical scales are identical throughout.

dx.doi.org/10.1021/jo201360u | J. Org. Chem. 2012, 77, 1258−1266

of dendrimer is indicative of the presence of complex equilibria in solution. The fluorescence intensity data is presented both as a function of the equivalents of dendrimer added (i.e., the ratio of the total stoichiometric concentrations of dendrimer and dye for each titration point) and as a function of the total concentration of ammonium groups added ([D]/[CF] multiplied by the number of surface positive charges for each dendrimer, see Table 1).

It is evident from the nonmonotonic trends in the titration isotherms that the fluorescence data cannot be explained simply by bound and unbound **CF** having two different optical states. Clearly, more than two binding regimes must exist with different optical properties in order to generate the inflections observed in the titration isotherms. Additionally, even though generational trends are still evident when plotting the observed changes as a function of the total concentration of ammonium groups (plots C and D in Figure 3), the differences in binding stoichiometry between dendrimer generations are significantly attenuated. This observation is in accordance with the assumption that electrostatic interactions play a pivotal role in dye binding. Further, the size of the macromolecular scaffold influences the degree of quenching and the rotational freedom of the complex (see below).

From these results, we postulate three coexisting states of interactions, whose relative importance is regulated by the dendrimer/dye ratio. First, at very low [dendrimer]/[**CF**] ratios, there is of course a large excess of **CF**, so the spectra are dominated by **CF** fluorescence, but each addition of dendrimer leads to extensive quenching. In fact, at approximately 0.03 equiv of **G7** dendrimer the most quenching is observed. This implies the loading of 33 **CF** per dendrimer at the point of maximum quenching. The high level of quenching should arise from not only the PET process with the dendrimer, but also from self-quenching due to a high local concentration of **CF** within the dendrimer. As more dendrimer is added, the **CF** molecules dynamically redistribute between dendrimers so that the contribution of the self-quenching process to the fluorescence signal decreases and only the PET quenching remains. Each lower generation of dendrimer shows progressively less self-quenching.

To further probe the sequestration of **CF** by the dendrimers, we analyzed fluorescence anisotropy. The anisotropy rises upon interaction of **CF** with the dendrimer as a consequence of the increased rotational correlation lifetime of the much heavier **CF**–dendrimer complexes (Figure 4A). However, close inspection of the region of the plot corresponding to low [dendrimer]/[**CF**] ratios reveals the presence of a plateau with each dendrimer, most evident with the higher generation dendrimers (Figure 4B).

For higher dendrimer generations a transition from a plateau to a rising hyperbola can be observed distinctly in the profile at low [dendrimer]/[**CF**]. With decreasing generations, however, the transition softens and the profile tends to assume a sigmoidal shape. Finally, the feature is blurred for **G4** but can still be made out as an irregularity in the profile. The plateaus and their transition to hyperbolic regions correspond to the same stoichiometry along the *x*-axis as the rapid quenching region, a dip, followed by a rise of emission in the fluorescence titrations (compare Figures 3B and 4B). Such considerations indicate that the underlying process must be linked with the size of the dendrimer molecules, which in turn led us to hypothesize that it also reflects stoichiometric properties of the dendrimer–dye aggregates.

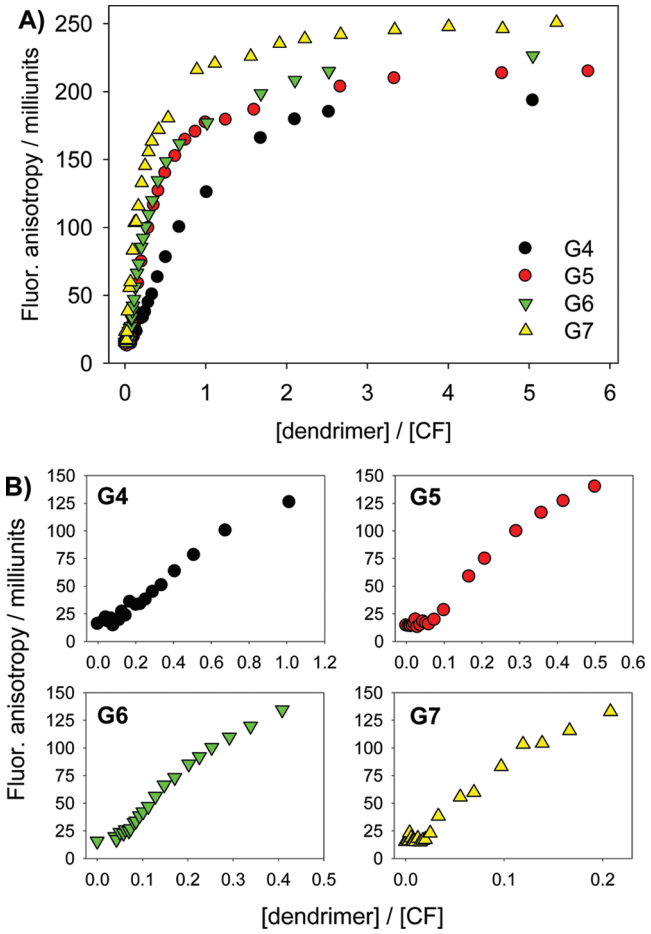

Figure 4. (A) Overlay of fluorescence anisotropy isotherms obtained during the course of titrations of solutions of 5(6)-carboxyfluorescein (**CF**) with **G4**–**G7** amine-terminated PAMAM dendrimer in buffered H_2O (50 mM HEPES at pH 7.4). [**CF**] = 2.0×10^{-6} M. (B) Details of the low [dendrimer]/[CF] region.

Interpretative Model of the Binding Interaction. In order to derive a model of the binding processes, it is instructive to compare the titration isotherms obtained from the different instrumental techniques. The Gröhn group recently reported binding studies for a family of sulfonated dyes to a G4 PAMAM dendrimer in water at pH 3.5. The reported UV–vis binding isotherms are monotonic square hyperbolas similar in nature to those we reported above. On the basis of that data and of ITC measurements, they proposed an interpretation of the binding process based on purely electrostatic forces and including dye–dye exciton interactions.[4c] Inspired by a similar approach but with the additional information obtained from the results of the luminescence experiments and from studies conducted across dendrimer generations, we propose here a general interpretative model capable of rationalizing the data and generational trends reported above. For convenience, we will exemplify our conclusions using data obtained for titrations executed with **G7** PAMAM because the relevant features are the most striking. However, our conclusions are general and take into account observed generational trends. Absorbance, fluorescence intensity, and anisotropy titration isotherms from a single titration of **CF** with **G7** dendrimer are presented overlaid in Figure 5. The plots have independent vertical scales that have been adjusted to aid comparison and highlight relevant features.

dx.doi.org/10.1021/jo201360u | *J. Org. Chem.* 2012, 77, 1258–1266

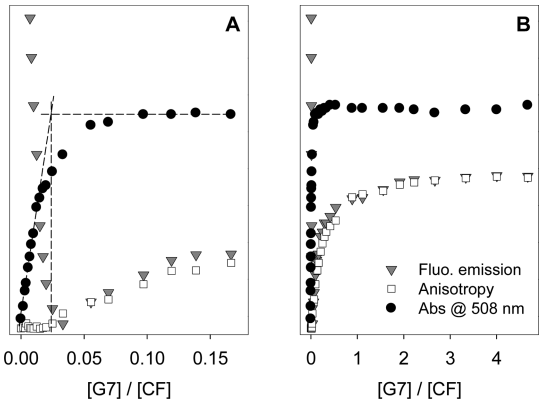

Figure 5. Overlay of absorbance, fluorescence intensity, and fluorescence anisotropy isotherms obtained from the same titration of 5(6)-carboxyfluorescein (**CF**) with **G7** PAMAM dendrimers. Vertical scales are adjusted to highlight profile similarities. (A) Detailed view of the low [**G7**]/[**CF**] region. (B) Complete titration. [**CF**] = 2.0×10^{-6} M in buffered H_2O (50 mM HEPES at pH 7.4).

As shown with dashed lines in Figure 5A, extrapolation of the vertical rise and the plateau region of the UV−vis profiles leads to an *x*-axis intercept of approximately 0.03 equiv of dendrimer, corresponding on average to 33 **CF** molecules aggregated together by the dendrimer. The saturation coincides with both the end of the plateau in the anisotropy profile and with the position of the tip of the trough in the fluorescence intensity profile. Beyond this point, the absorbance reaches saturation and no further change is observed with higher dendrimer equivalents, since **CF** will redistribute among dendrimers and generate smaller aggregates. These interactions are already completely established at low dendrimer ratios, i.e., in the presence of high-stoichiometry aggregates, and do not change fundamentally upon redistribution of the **CF** molecules as the concentration of dendrimer is increased during the course of the titration. In other words, at a first approximation the *absorption* properties seem to be independent of dye-to-dye interactions and to depend only on the dye-to-dendrimer interaction.

As already indicated, within the dendrimer concentration range in which the binding of **CF** is occurring according to the absorbance and fluorescence titration, the fluorescence anisotropy profile is relatively flat. This could signify either that no binding is taking place, or that binding occurs with no accompanying change in anisotropy signal. On the basis of the data of Figures 1−3, we propose the latter explanation. The high stoichiometry of the aggregates must be the cause of the lack of an anisotropy increase, even when binding is occurring. The dendrimers sequester the fluorophores at a close distance to each other, thus allowing significant and possibly unexpected electronic interactions between them to occur.

In the particular case of fluoresceins, the small Stokes shift typical of these fluorophores facilitates nonradiative resonant energy transfer (RET), also known as self-quenching.[9] The Förster radius for fluorescein RET homoexchange is 44 Å,[10] which is compatible with the range of distances foreseeable between the dendrimer-bound fluorescent molecules in a high-stoichiometry complex (see Table 1). This process is particularly effective at scrambling the polarization of the emitted fluorescence and is therefore responsible for the initial flat portion of the anisotropy titration profile. It is known that each single step of RET reduces the recovered anisotropy to only 4% of its initial value.[10] The anisotropy signal starts rising as the dendrimer concentration is increased past the region where high-stoichiometry complexes prevail, reflecting the fact that the **CF** molecules redistribute to lower stoichiometry complexes.

In the context of the present study, a population of fully dendrimer-bound, slowly rotating fluorophores undergoing RET thus emit light with extremely low polarization, as though they were still freely rotating in the bulk solution. These considerations allow us to reconcile the information obtained from the absorbance, fluorescence, and the fluorescence anisotropy profiles in the region of very low [dendrimer]/[**CF**]. In fact, the very same proximity effects and connected RET process that explain the polarization scrambling also provide an explanation for the initial precipitous decline in the fluorescence emission as arising from self-quenching. Indeed, the efficient self-quenching property of fluorescein and its derivatives in concentrated solutions (mM) is well-known.[11] By extension, it is reasonable to assume that in the high-stoichiometry complexes the **CF** molecules undergo a similar self-quenching process due to their close proximity imposed by dendrimer binding.

In summary, we found three coexisting regimes, whose relative importance is regulated by the [dendrimer]/[**CF**] ratio. At extremely low [dendrimer]/[**CF**] ratios, most of the dye molecules are still free in solution, a state characterized by absorbance spectra typical of the free anionic fluorophore in solution, high fluorescence emission, and low anisotropy. A small increase in the [dendrimer]/[**CF**] ratio favors the formation of high-stoichiometry dendrimer−**CF** complexes. The ammonium groups on the dendrimer engage in electrostatic and potentially cation-π interactions with the aromatic moieties in the dye, yielding a corresponding change in absorbance. At the same time, the forced proximity of the **CF** molecules induces RET, which in turn provides for very efficient quenching of the fluorescence intensity and polarization scrambling. Finally, increasing the dendrimer concentration favors the formation of lower stoichiometry adducts and eventually the formation of 1:1 dendrimer−**CF** adducts in the region of high [dendrimer]/[**CF**] ratios. The nature of the dendrimer−**CF** interaction in these adducts is essentially the same as that observed in the low stoichiometry adducts, as testified by the early saturation of the absorbance profile. Also, in these adducts the **CF** molecules find themselves further apart and eventually are completely isolated, each in their own dendrimer. Thus, the efficiency of the RET process declines and the fluorescence intensity signal climbs up toward its final value, while the fluorescence anisotropy also rises to saturation. In this regime, these two signals are linked by their dependence on the RET process and dendrimer quenching, and on the molar fraction of **CF** present as low-stoichiometry adducts. Ultimately, the formation of complexes with 1:1 **CF**−dendrimer stoichiometry leads to saturation of all signals.

Modeling the High-Stoichiometry Aggregation. In order to evaluate the plausibility of our model, we tested it in a simulated titration. We used a relatively simple simulated binding system comprising two species and seven binding equilibria, as outlined in eq 2. This is clearly simpler than the system under study that predicts stoichiometries in the range of 30 or more equilibria; however, we propose that it is complex enough to provide valuable qualitative insight. Indeed, we only attempted to reproduce the trends observed in the experimental data qualitatively, and we will not attempt quantitative prediction or use of the model for curve fitting. The model reported does not directly apply to any dendrimer generation in

specific, but we will show that it does reproduce trends observed in all generations. Values have been assigned arbitrarily to the formation constants, taking into account **CF**-to-**CF** repulsion in the higher stoichiometry complexes.

$$\begin{cases} D + CF \rightleftharpoons [D{\cdot}CF] & (\log K_1 = 8.0) \\ [D{\cdot}CF] + CF \rightleftharpoons [D{\cdot}CF_2] & (\log K_2 = 8.0) \\ [D{\cdot}CF_2] + CF \rightleftharpoons [D{\cdot}CF_3] & (\log K_3 = 7.5) \\ [D{\cdot}CF_3] + CF \rightleftharpoons [D{\cdot}CF_4] & (\log K_4 = 7.0) \\ [D{\cdot}CF_4] + CF \rightleftharpoons [D{\cdot}CF_5] & (\log K_5 = 6.5) \\ [D{\cdot}CF_5] + CF \rightleftharpoons [D{\cdot}CF_6] & (\log K_6 = 6.0) \\ [D{\cdot}CF_6] + CF \rightleftharpoons [D{\cdot}CF_7] & (\log K_7 = 5.5) \end{cases} \quad (2)$$

The equilibrium concentrations of all relevant species during the course of a simulated titration were calculated numerically through the Hyss2009 program,[12] assuming a constant concentration of **CF** throughout the titration ([**CF**] = 2.0×10^{-6} M, equal to that used in the experimental titrations) and varying the dendrimer concentration over the range 0–6.0×10^{-6} M, which corresponds to [dendrimer]/[**CF**] = 0–3 (also a typical value used in the experimental studies presented above).

In order to simulate the experimental isotherms, we estimated reasonable intrinsic anisotropies and relative quantum efficiencies for each fluorescent species present at equilibrium. In particular, according to our proposed model the fluorescent species may be grouped in three categories: (**a**) the mole fraction of fluorophore **CF** free in solution, with high fluorescence intensity and low anisotropy (χ_a); (**b**) the mole fraction of low stoichiometry complexes, here identified as the 1:1 and 1:2 fluorophore:dendrimer complex [**D**·**CF**] and [**D**·**CF**$_2$], free from RET interactions and therefore characterized by partially quenched fluorescence emission and high anisotropy (χ_b); and (**c**) the mole fraction of higher stoichiometry complexes, here [**D**·**CF**$_3$], [**D**·**CF**$_4$], [**D**·**CF**$_5$], [**D**·**CF**$_6$], [**D**·**CF**$_7$], in which RET interactions are strong, with the consequences of almost completely quenched fluorescence emission and very low anisotropy (χ_c).

Molar fractions relative to the total fluorophore concentration were calculated as shown in eqs 3, 4, and 5 for each of the three categories introduced above, from the molar concentrations of the participating species obtained from the simulated binding model for each titration point. From these values, the simulated absorbance (Abs), fluorescence emission (normalized) (I_F/I_0), and anisotropy titration profiles (r_{sol}), were then calculated as shown in eqs 6, 7, and 8, respectively.

$$\chi_{\mathbf{a}} = \chi_{CF} = \frac{[CF]}{[CF]_{tot}} \quad (3)$$

$$\chi_{\mathbf{b}} = \chi_{[D\cdot CF]} + \chi_{[D\cdot CF_2]} = \frac{[D\cdot CF] + 2[D\cdot CF_2]}{[CF]_{tot}} \quad (4)$$

$$\chi_{\mathbf{c}} = \sum_{7}^{i=3} \chi_{[D\cdot CF_i]} = \sum_{7}^{i=3} \frac{i[D\cdot CF_i]}{[CF]_{tot}} \quad (5)$$

$$\text{simulated } I_F/I_0 = \Phi_{\mathbf{a}}^{rel}\chi_{\mathbf{a}} + \Phi_{\mathbf{b}}^{rel}\chi_{\mathbf{b}} + \Phi_{\mathbf{c}}^{rel}\chi_{\mathbf{c}} \quad (6)$$

$$\text{simulated } r_{sol} = r_{\mathbf{a}}^{intr}\chi_{\mathbf{a}} + r_{\mathbf{b}}^{intr}\chi_{\mathbf{b}} + r_{\mathbf{c}}^{intr}\chi_{\mathbf{c}} \quad (7)$$

$$\text{simulated Abs}_{508nm} = 0.040\chi_{\mathbf{a}} + 0.105(\chi_{\mathbf{b}} + \chi_{\mathbf{c}}) \quad (8)$$

The numerical values for the optical properties assumed for each of these mole fractions are presented in Table 2.

Table 2. Parameters Used in the Calculation of Simulated Absorbance, Fluorescence Emission, and Anisotropy Titration Profiles Based on the Species Distributions[a]

group	species	Φ^{rel}	r^{intr}	Abs (508 nm)
a	**CF**	1.0 (ref)	13 (m)	0.040 (m)
b	[**D**·**CF**], [**D**·**CF**$_2$]	0.35 (m)	250 (m)	0.105 (m)
c	[**D**·**CF**$_3$] → [**D**·**CF**$_7$]	0.05 (est)	25 (est)	0.105 (m)

[a] Φ^{rel} = fluorescence emission quantum efficiency, relative to the free CF fluorophore in solution. r^{intr} = intrinsic anisotropy value (milliunits) for the species. Abs (508 nm) = absorbance at 508 nm for the species. (rel) indicates a value used as a reference. (est) indicates an estimate based on qualitative predictions from our proposed interaction model. (m) indicates experimental values obtained from direct measurement. 0.040 is an intrinsic property of the free fluorophore in our experimental conditions; the 0.105 value was estimated by averaging the absorbance end points of the dendrimer titrations throughout all generations.

Normalized fluorescence intensities (Φ^{rel}) were calculated relative to the fluorescence of free **CF** in our experimental conditions (2.0×10^{-6} M in aqueous 50 mM HEPES at pH 7.4), which was set to 1. The relative fluorescence intensity (Φ^{rel}), anisotropy (r^{intr}), and absorbance at 508 nm for fraction **a** (free **CF**) are intrinsic properties of the **CF** fluorophore in our experimental conditions; these can be derived from the first points of the titration profiles. The optical properties (Φ^{rel}, r^{intr}, Abs at 508 nm) for fraction **b** (bound **CF**, no self-interactions) are also experimentally derived values, taken to correspond to the average values across all dendrimer generations of the optical properties of solutions containing a high [dendrimer]/[**CF**] ratio. Numerical values were obtained from solutions containing a 20:1 [dendrimer]/[**CF**] ratio for dendrimers **G4**–**G7**. These solutions were not prepared independently but actually correspond to the last points (i.e., high dendrimer concentration) of the titrations presented above. However, in the figures shown throughout this paper most titration isotherms were shown only to a maximum of 5:1 [dendrimer]/[**CF**] ratio to enhance detail.

The relative fluorescence intensity (Φ^{rel}) and anisotropy (r^{intr}) for fraction **c** are reasonable estimates based on the behavior postulated by our model. For instance, it is known[9−11] that quenching of the fluorescence and scrambling of the anisotropy due to RET are both very efficient in xanthene fluorophores, so the relative fluorescence intensity (Φ^{rel}) was assumed to be only 5% of the natural fluorescence of the free **CF** fluorophore. Likewise, the intrinsic anisotropy (r^{intr}) was assumed to rise only slightly above that measured for the free

dx.doi.org/10.1021/jo201360u | J. Org. Chem. 2012, 77, 1258–1266

CF fluorophore. Moreover, the absorbance at 508 nm for this fraction was set to the same value as that for fraction **b**, in accordance with our proposed model. In fact, we postulate that once binding has taken place the absorbance signal is insensitive to further changes in stoichiometry, so all forms of bound **CF** will have the same absorbance contribution independent of stoichiometry.

The results from the simulation using the parameters just discussed are presented in Figure 6. The species distribution for

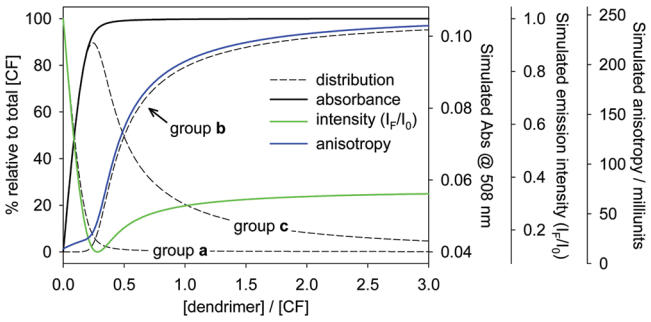

Figure 6. Simplified model of the dendrimer−**CF** interaction: calculated species distributions (dotted lines, as percentages relative to total **CF**) and simulated experimental responses (solid lines) for absorbance (black), fluorescence intensity (blue) and fluorescence anisotropy (green).

each of the three groups (dotted lines) confirms that this model system can simulate the proposed uptake of **CF** by the dendrimers (**D**). The initial products of complexation are high-stoichiometry complexes, while an increase in dendrimer concentration then favors the formation of the [**D**·**CF**] 1:1 species, which coexists in solution with an excess of free dendrimer. The shape of the distribution profile for the group **b** species ([**D**·**CF**] and [**D**·$\mathbf{CF_2}$]) is also noteworthy, in that it contains an initial plateau at low [dendrimer]/[**CF**] ratios.

Isothermal Titration Calorimetry. Given the high-stoichiometry binding of **CF** to the PAMAM dendrimers, we chose to further pursue the study of the binding via isothermal titration calorimetry (ITC). By using ITC, we were able to estimate binding stoichiometry, measure binding constants, and obtain thermodynamic information about the binding events. To this extent, we studied the binding of **CF** to **G3**−**G6** PAMAM dendrimers. The **G7** PAMAM dendrimer was not included in this study, because the generation was too expensive to obtain the necessary concentrations to acquire acceptable ITC data.

According to previous reports,[13] the dilution of PAMAM dendrimers gives large ITC signatures, and thus a constant concentration of dendrimer was used in each experiment with **CF** used as the titrant. The titrations gave a consistent exponential increase in the equivalents of **CF** bound per generation of dendrimer (reflected by ITC n values) as expected on the basis of the exponential increase in both size and charge through the generations (one example is given in Figure 7). As shown in Table 3, the amount of **CF** bound increases from

Table 3. ITC Data for G3−G6 AT-PAMAM Dendrimers

generation	n	binding constant (M^{-1})	enthalpy (cal/mol)	entropy (eu)
G3	2.4 ± 0.1	3100 ± 100	−6700 ± 300	−6.03
G4	8.5 ± 0.1	2600 ± 90	−6800 ± 100	−6.64
G5	21.8 ± 0.2	2300 ± 100	−6100 ± 100	−4.64
G6	50.2 ± 0.3	2020 ± 70	−5870 ± 50	−4.23

2.4 ± 0.1 for generation 3 to 50.2 ± 0.3 for generation 6. These values come from the curve fitting routine, and we do not place much stock in them. In fact, the stoichiometry is extremely high, and therefore we believe the trends are more relevant than the actual values.

Given the model used in the ITC, we found that the binding constant for **CF** decreases as dendrimer generation increases, from 3100 ± 100 M^{-1} for generation 3 to 2020 ± 70 M^{-1} for generation 6. The binding constants reported are calculated from the Gibbs free energy change ($\Delta G°$) of the solution as measured by ITC.

Finally, given that the thermodynamic values are very similar for each of the dendrimer generations, they likely reflect the notion that the dendrimers bind **CF** using similar binding modes. As can be seen in Table 3, the ΔH values are all very similar at approximately −6 kcal/mol, while the ΔS values vary between −6.6 to −4.2 eu. The negative ΔH values indicate a

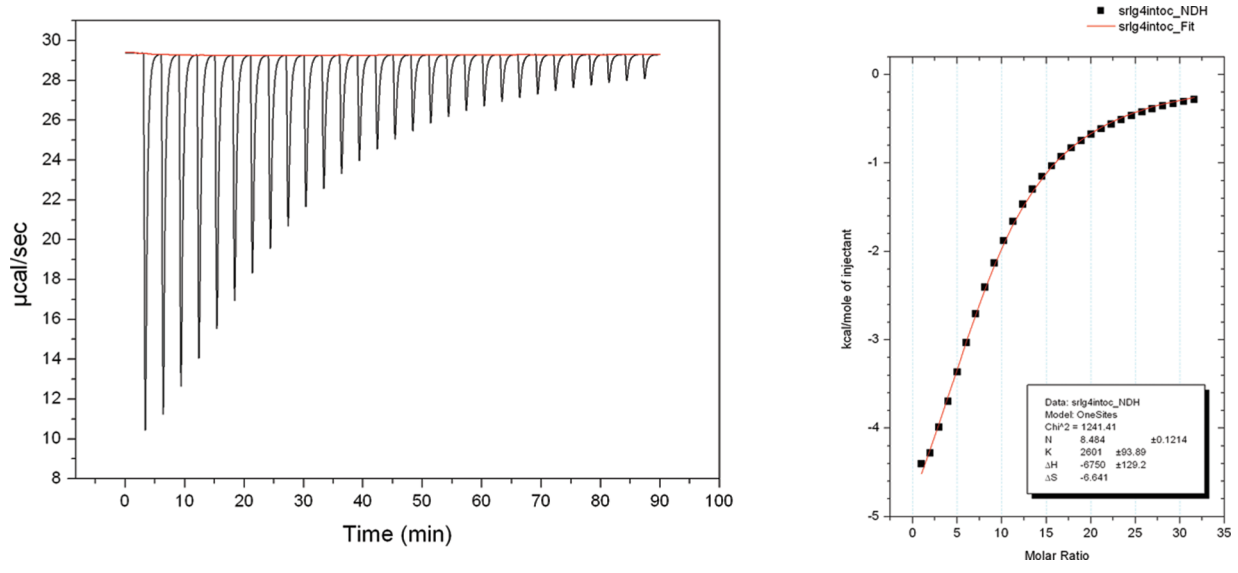

Figure 7. Raw ITC isotherm and the processed isotherm with the fit for the titration of **CF** into dendrimer (**G4**).

dx.doi.org/10.1021/jo201360u | J. Org. Chem. 2012, 77, 1258−1266

net exothermic contribution potentially derived from electrostatic binding interaction, with higher generations showing slightly lower ΔH values, while the negative entropy values are supportive of the idea that multiple indicators are binding to form one larger complex, thus increasing the order of the system. However, this effect would be counterbalanced by the release of dendrimer counteranions into solution.

Once we had spectral and ITC data we could calculate the maximum binding stoichiometry in three different ways (Table 4).

Table 4. Stoichiometry of Binding Extrapolated from Multiple Methods

generation	absorbance	fluorescence intensity	isothermal titration calorimetry
G3	N/A	N/A	2
G4	4	4	8
G5	7	7	21
G6	12	12	50
G7	33	33	N/A

Plotting the absorbance versus the concentration of dendrimer added, we were able to construct a pseudobinding isotherm. By extrapolating the initial rise of the absorbance data and the plateau to a point of intersection,[5] we were able to estimate the binding stoichiometry. A similar procedure was utilized with the fluorescence intensity measurements, but the ratio was based upon the intersection of the rise in the fluorescence intensity with the plateau, rather than utilizing any of the dip structure found in the isotherm. For the stoichiometry obtained from the ITC measurements, the n values that were provided from the one site model were used for comparison.

While the absorbance and fluorescence intensity measurements strongly agree in the ratio of **CF** to dendrimer binding, the ITC measurements show a significantly higher ratio of binding. The discrepancy may be due to the inherent cumulative nature of the ITC data, which necessarily reports on all molecular interactions involved in the binding process, whereas the spectroscopic investigations report only on the environment of the **CF**. Although a discrepancy exists in the actual numbers for the stoichiometry of binding arising from the optical and ITC data, the trends are clear. An exponential increase in the ability of dendrimer generations to uptake **CF** exists. The higher generation dendrimers can clearly sequester together dozens of anionic indicators, which sets the stage for controlled high-stoichiometry assembly processes.

CONCLUSIONS

In this paper, the dynamics of binding between **CF** and PAMAM dendrimer were explored using both optical and calorimetric techniques. Using the spectroscopic techniques, a binding ratio between the anionic indicator and the cationic dendrimer was determined. Most importantly, the optical techniques provided valuable information about the mechanisms of optical modulation during the binding event. First, as dendrimer is added, aggregation of **CF** and PET quenching cause a rapid decrease in the fluorescence intensity. As more dendrimer is added, the self-quenching from aggregation is reduced and thus an increase in fluorescence intensity is seen. After this increase, the intensity levels out. Similarly, as the prevalence of the RET process decreases, fluorescence anisotropy is free to increase as the **CF** is bound to the dendrimer, and the rate at which the fluorophore tumbles in solution is reduced.

Further studies with isothermal titration calorimetry provided thermodynamic details of the binding between **CF** and the dendrimers in solution. Each of these studies showed that the binding of **CF** to the cationic dendrimers is reversible, allowing for the binding of a large number of anionic charges and showing a significant signal modulation. Further studies exploring this signaling method are underway in our lab.

EXPERIMENTAL SECTION

General Conditions. Poly(amidoamine) (PAMAM) dendrimers with ethylenediamine core and primary amine surface group termination were used in these studies. The dendrimers were manufactured by Dendritech and distributed by Sigma-Aldrich as MeOH solutions. Dendrimer solutions were stored refrigerated at 4 °C and used as received. The fluorescent probe 5(6)-carboxyfluorescein (mixture of isomers) was obtained from Sigma and used as received.

All reported optical spectroscopy experiments were carried out on a Biotek Synergy 2 multimode plate reader, capable of measuring absorbance spectra (through a monochromator) and steady-state fluorescence intensity and anisotropy (through bandpass filter sets and plastic sheet polarizers). Experiments were laid out by hand using Eppendorf Research multichannel pipettors and disposable plastic tips into Corning 96-well nontreated (medium-binding) polystyrene plates with black walls and clear flat bottoms.

All experiments on dendrimer generations **G4**, **G5**, and **G7** were carried out using the same dendrimer commercial stock solution, whereas **G6** experiments were conducted from two lots of dendrimer. In the latter case we confirmed lot-to-lot consistency by successfully replicating a number of **G6**–fluorophore interaction experiments on both lots. In general, all experiments were carried out in aqueous solutions buffered to pH 7.4 with 4-(2-hydroxyethyl)-1-piperazineethanesulfonic acid (HEPES, 50 mM).

Dendrimer content in commercial stock solutions is characterized as percent by weight (from certificate of analysis of each lot). In order to manipulate the solutions more readily in our titration experiments, their molar concentration was needed. Therefore, we determined the density of all stock dendrimer solutions experimentally by repeatedly dispensing small volumes of each solution into a small septum-sealed vial using a Hamilton GASTIGHT cemented-needle syringe and weighing the aliquots (see Chart S1 in Supporting Information).

Binding Isotherms. In a typical binding study, a titration isotherm was constructed point by point, by laying out a number of solutions containing increasing [dendrimer]/[fluorophore] ratios across a multiwell plate. The concentration of the fluorophore was kept constant at 2.0×10^{-6} M throughout the experiment. The total volume of solution in the microwell (300 μL) was also kept constant, as this parameter controls the height of liquid in the wells and therefore the optical path length in the experiment.

Most experiments were laid out entirely on a single plate, in order to minimize plate-to-plate variations. A few binding experiments requiring wider [dendrimer]/[fluorophore] ranges were conducted on multiple plates. In those cases selected data points (generally the free fluorophore, the midpoint, and the end point of the titration) were replicated through all plates in order to ascertain consistency. Each data point was replicated a minimum of two times on each plate, and each full experiment was run at least twice to ensure reproducibility.

We found that minimizing the number of additions per well significantly increased the precision of our measurements. In order to do so, for each experiment we prepared two sets of solutions, both of which contained **CF** at the final working concentration of 2.00×10^{-6} M; dendrimer was added to one set only (see Supporting Information). Mixing variable amounts of dendrimer-free and dendrimer-containing solutions in the microplate wells allowed us to attain a wide range of [dendrimer]/[fluorophore] ratios with only two dispenses.

Manual dispensing of solutions into each plate generally required less than 30 min, and in that time no significant evaporation was

dx.doi.org/10.1021/jo201360u | J. Org. Chem. 2012, 77, 1258–1266

observed. Plates were read in a multimode plate reader immediately after preparation. Absorbance spectra, nonpolarized fluorescence emission, and polarized fluorescence anisotropy data were acquired, in that order. Reading time was roughly 45 min per plate. Full absorbance spectra (410−560 nm) were recorded. Steady-state fluorescence intensity readings were obtained through a 485/20 nm and a 540/25 nm filter set for excitation and emission respectively. In the case of fluorescence, automatic detector gain adjustment was used, so that the highest reading from each plate (invariably that of the free fluorophore wells) reached 85% of the instrument full scale. Each reported fluorescence intensity data point (i.e., the value reported for each well) was the average of 10 readings. Sheet polarizers were installed in the machine for the determination of emission anisotropy.

Both absorbance and fluorescence emission raw readings were blanked by subtracting the corresponding average reading for the 12 wells containing neat buffer, and then replicate data points were averaged. Moreover, the factory-determined *g*-factor for our instrument (0.87) was used when calculating the fluorescence emission anisotropy from the parallel- and perpendicular-polarized emission readings. Finally, fluorescence emission data was normalized by dividing by the emission of the free **CF** fluorophore in each plate (invariably the highest measured in these experiments) for readability. Data was plotted as a function of [dendrimer]/[**CF**] ratio to produce binding isotherms.

ITC. All ITC measurements were obtained using a VP-ITC calorimeter from MicroCal, a division of GE Healthcare (Piscataway, New Jersey). The AT-PAMAM dendrimer (as a methanol solution) and 5(6)-carboxyfluorescien were purchased from Aldrich and used as received. 4-(2-Hydroxyethyl)-1-piperazineethanesulfonic acid (HEPES) (Molecular Biology grade) was purchased from Fisher and used to prepare a 250 mM buffer solution in millipure water at pH 7.4. The pH of each solution was measured and adjusted if needed to ensure there were no fluctuations in the pH occurred upon the addition of **CF** or dendrimer. The concentration of dendrimer was kept constant in both the cuvette and titrant solutions at 100 μM for **G3**−**G5** and 50 μM for **G6**. The titrant solution contained 14 mM **CF** (for **G3** and **G4**) and 21 mM **CF** (for **G5** and **G6**) that was injected from a 300 μL syringe. The cuvette was filled with approximately 1.4 mL of a buffered dendrimer solution. To this solution, the titrant solution was added in 10 μL aliquots for a total of 30 injections with 180 s spacing, a 180 s initial delay and a 10.3 s injection duration with stirring of 260 rpm. After the titration, the pH of the solution was again measured to ensure that there was no change in pH during the titration.

The raw ITC data was fit using a one binding site model because it gave the best fit of the data. This model treats each **CF** binding to the PAMAM dendrimer as having the same thermodynamic properties. We felt this assumption was reasonably valid because each **CF** should bind with a similar electrostatic interaction. While this approach likely inflated the thermodynamic properties of the later bound **CF** and underestimated the earliest equivalents of **CF**, this trade-off would balance to some extent.

■ ASSOCIATED CONTENT

Ⓢ Supporting Information

This material is available free of charge via the Internet at http://pubs.acs.org.

■ AUTHOR INFORMATION

Corresponding Author

*E-mail: anslyn@austin.utexas.edu.

■ ACKNOWLEDGMENTS

This work was supported by the National Science Foundation (CHE-06106467) and the Welch Foundation (F-1151).

■ REFERENCES

(1) (a) Chen, B.; Xiang, S.; Qian, G. *Acc. Chem. Res.* **2010**, *43*, 1115−1124. (b) Mancin, F.; Scrimin, P.; Tecilla, P.; Tonellato, U. *Coord. Chem. Rev.* **2009**, *253*, 2150−2165. (c) Pluth, M. D.; Bergman, R. G.; Raymond, K. N. *Acc. Chem. Res.* **2009**, *42*, 1650−1659.

(2) Niu, Y.; Sun, L.; Crooks, R. M. *Macromolecules* **2003**, *36*, 5725−5731.

(3) Cakara, D.; Kleimann, J.; Borkovec, M. *Macromolecules* **2003**, *36*, 4201−4207.

(4) (a) Klajnert, B.; Pastucha, A.; Shcharbin, D.; Bryszewska, M. *J. Appl. Polym. Sci.* **2007**, *103*, 2036−2040. (b) McHedlov-Petrossyan, N. O.; Bryleva, E. Y.; Vodolazkaya, N. A.; Dissanayake, A. A.; Ford, W. T. *Langmuir* **2008**, *24*, 5689−5699. (c) Willerich, I.; Ritter, H.; Gröhn, F. *J. Phys. Chem. B* **2009**, *113*, 3339−3354.

(5) Rainwater, J. C.; Anslyn, E. V. *Chem. Commun.* **2010**, *46*, 2904−2906.

(6) Aschi, M.; D'Archivio, A. A.; Fontana, A.; Formiglio, A. *J. Org. Chem.* **2008**, *73*, 3411−3417.

(7) The M_w, diameter, and number of surface NH_2 groups were taken from literature on the manufacturer's website (Dendritech, www.dendritech.com/pamam, accessed on 02/25/2011).

(8) (a) Dougherty, D. A.; Stauffer, D. A. *Science* **1990**, *250*, 1558. (b) Ma, J. C.; Dougherty, D. A. *Chem. Rev.* **1997**, *97*, 1303.

(9) (a) Weber, G.; Shinitzky, M. *Proc. Natl. Acad. Sci. U.S.A.* **1970**, *65* (4), 823−30. (b) Van der Meer, B. W.; Coker, G.; Chen, S. Y. S. *Resonance Energy Transfer: Theory and Data*; VCH: New York, 1994. (c) Walter, B. *Ann. Phys.* **1888**, *270*, 316−26. (d) Chen, R. F.; Knutson, J. R. *Anal. Biochem.* **1988**, *172*, 61−77.

(10) (a) Lakowicz, J. R. *Principles of Fluorescence Spectroscopy*, 3rd ed.; Springer: New York, NY, 2006. (b) Kalinin, S.; Molotkovsky, J. G.; Johansson, L. B. A. *J. Phys. Chem. B* **2003**, *107*, 3318−3324. (c) Baumann, J.; Fayer, M. D. *J. Chem. Phys.* **1986**, *85*, 4087−4107.

(11) Hamann, S.; Kiilgaard, J. F.; Litman, T.; Alvarez-Leefmans, F. J.; Winther, B. R.; Zeuthen, T. *J. Fluoresc.* **2002**, *12*, 139−145.

(12) Alderighi, L.; Gans, P.; Ienco, A.; Peters, D.; Sabatini, A.; Vacca, A. *Coord. Chem. Rev.* **1999**, *184*, 311−3118.

(13) Yang, W; Li, Y; Cheng, Y; Wu, Q; Wen, L; Xu, T *Pharm. Nanotechnol.* **2009**, *98* (3), 1075−1085.